GEOPHYSICAL RESEARCH LETTERS, VOL. 38, L17107, doi:10.1029/2011GL048671, 2011

The properties of large amplitude whistler mode waves in the magnetosphere: Propagation and relationship with geomagnetic activity

L. B. Wilson III,[1,2] C. A. Cattell,[2] P. J. Kellogg,[2] J. R. Wygant,[2] K. Goetz,[2] A. Breneman,[2] and K. Kersten[2]

Received 24 June 2011; revised 11 August 2011; accepted 11 August 2011; published 9 September 2011.

[1] We present results of a study of the characteristics of very large amplitude whistler mode waves inside the terrestrial magnetosphere at radial distances of less than 15 R_E using waveform capture data from the Wind spacecraft. We observed 247 whistler mode waves with at least one electric field component (105/247 had ≥80 mV/m peak-to-peak amplitudes) and 66 whistler mode waves with at least one search coil magnetic field component (38/66 had ≥0.8 nT peak-to-peak amplitudes). Wave vectors determined from events with three magnetic field components indicate that 30/46 propagate within 20° of the ambient magnetic field, though some are more oblique (up to ~50°). No relationship was observed between wave normal angle and GSM latitude. 162/247 of the large amplitude whistler mode waves were observed during magnetically active periods (AE > 200 nT). 217 out of 247 total whistler mode waves examined were observed inside the radiation belts. We present a waveform capture with the largest whistler wave magnetic field amplitude (≳8 nT peak-to-peak) ever reported in the radiation belts. The estimated Poynting flux magnitude associated with this wave is ≳300 $\mu W/m^2$, roughly four orders of magnitude above estimates from previous satellite measurements. Such large Poynting flux values are consistent with rapid energization of electrons. **Citation:** Wilson, L. B., III, C. A. Cattell, P. J. Kellogg, J. R. Wygant, K. Goetz, A. Breneman, and K. Kersten (2011), The properties of large amplitude whistler mode waves in the magnetosphere: Propagation and relationship with geomagnetic activity, *Geophys. Res. Lett.*, *38*, L17107, doi:10.1029/2011GL048671.

1. Introduction

[2] Whistler mode waves are one of the most ubiquitous wave modes observed in space plasmas. They have been observed in the magnetosphere [*Burtis and Helliwell*, 1969], in the solar wind [*Neubauer et al.*, 1977], upstream of interplanetary shocks [*Wilson et al.*, 2009], upstream of planetary bow shocks [*Hoppe et al.*, 1981], and in cometary foreshocks [*Tsurutani et al.*, 1987]. Whistler mode waves are a right-hand polarized electromagnetic mode that can propagate along the magnetic field, obliquely to the magnetic field, or nearly perpendicular to the magnetic field as a quasi-electrostatic mode near the resonance cone [*Bell and Ngo*, 1990]. For simplicity, we will not distinguish between chorus, plasmaspheric hiss, or oblique whistler-modes in our use of the term whistler mode wave. In the magnetosphere, whistler mode waves are thought to be driven unstable by electron temperature anisotropies [*Kennel and Petschek*, 1966]. Because whistler mode waves interact strongly with energetic particles [*Kennel and Petschek*, 1966; *Lyons et al.*, 1972], it has been well accepted that they play an important role in global radiation belt dynamics. Thus, whistler mode waves have been a topic of extreme interest for over 40 years in magnetospheric physics.

[3] For the past 30 years plasma wave measurements have primarily consisted of time-averaged spectral intensity data. Typical time-averaged spectral zero-to-peak amplitudes for whistler mode waves are ~0.5 mV/m for the electric field [*Meredith et al.*, 2001] and ~0.01–0.1 nT for the magnetic field [*Horne et al.*, 2003, 2005]. *Tsurutani et al.* [2009] showed that time-averaged spectral amplitudes can severely underestimated the instantaneous wave amplitudes. This discrepancy was exemplified with the discovery of very large amplitude (>200 mV/m) whistler mode waves in the radiation belts using the STEREO spacecraft [*Cattell et al.*, 2008], and in later observations by the Wind [*Kellogg et al.*, 2011] and THEMIS [*Cully et al.*, 2008] spacecraft. *Cattell et al.* [2008] also showed that these waves were capable of energizing electrons by more than an MeV in less than a second, which is consistent with test particle simulations [*Omura et al.*, 2007; *Bortnik et al.*, 2008]. Furthermore, recent observations have shown evidence that these large amplitude whistler mode waves are capable of trapping [*Kellogg et al.*, 2010] and prompt scattering into the loss-cone of radiation belt particles [*Kersten et al.*, 2011]. These observations have raised new questions regarding the energization and lifetime of radiation belt particles.

[4] During an eight year period, the Wind spacecraft went through a number of petal orbits within the terrestrial magnetosphere. We report on whistler mode wave observations for 13 of those petal orbits, building on the study by *Kellogg et al.* [2011], who used an automated search algorithm that only examined a subset of the available waveform captures to find whistler mode waves. We examined all of the waveform captures and obtained significantly more whistler mode waves. The paper is organized as follows: Section 2 introduces and outlines the data sets and analysis techniques, Section 3 describes the observations, and Section 4 discusses the conclusions of our study.

2. Data Sets and Analysis

[5] Waveform captures were obtained from the Wind/WAVES instrument [*Bougeret et al.*, 1995], using the time

[1]NASA Goddard Space Flight Center, Greenbelt, Maryland, USA.
[2]School of Physics and Astronomy, University of Minnesota, Twin Cities, Minneapolis, Minnesota, USA.

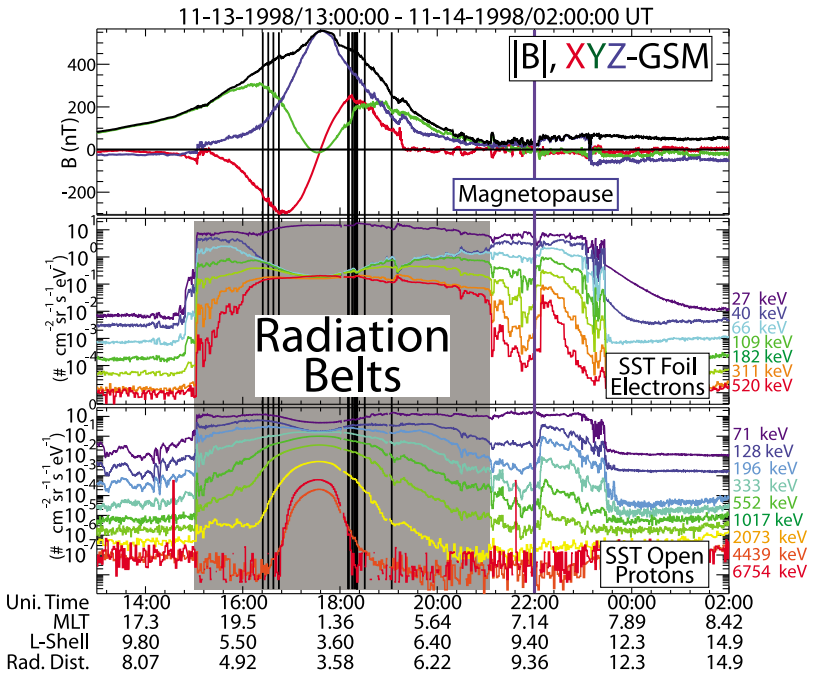

Figure 1. Example of a Wind petal orbit for the time range of 1998-11-13/13:00:00 UT through 1998-11-14/02:00:00 UT. (top) The GSM components of the magnetic field and magnitude. (middle and bottom) Omni-directional number fluxes of high energy electrons (SST Foil) and protons (SST Open), respectively, from the Wind/3DP instrument. At the bottom of the plot are tick mark labels of MLT, L-Shell, and radial distance along with the local UT. The vertical black lines correspondto TDS samples identified as whistler mode waves. The radiation belts are shown by the shaded region and the magnetopause crossing by the vertical blue line near 22:00 UT. The five lowest energy bins for the SST Foil and three lowest for the SST Open plots show a decrease in flux as Wind reaches perigee. This is not physical and is identified as saturation of detector at these energies [*McFadden et al.*, 2007].

domain sampler (TDS) receiver, which provides a waveform capture (herein called TDS sample) of 2048 points with timespans ranging from ~17 ms to ~1000 ms, depending on sample rate. The TDS receiver has both a fast (TDSF) and slow (TDSS) receiver. The TDSF receiver returns two electric field components in the spacecraft spin plane (roughly the XY-GSE plane), while the TDSS receiver returns four vector components, either three electric and one magnetic or vice versa. A more detailed description of the TDS onboard memory buffer and evaluation criteria is given by *Kellogg et al.* [2011]. We also add that the TDS instrument continuously returns both the most recent and the best quality (typically defined by amplitude) waveform in its telemetry stream. The best quality waveforms receive more telemetry and thus bias the transmitted waveform captures to larger amplitude waves. All the amplitudes reported herein will be peak-to-peak.

[6] We use the Wind/3DP [*Lin et al.*, 1995] solid state telescopes (SSTs) to identify the periods when Wind entered (exited) the radiation belts, defined by the sharp increase (decrease) in omni-directional flux of the high energy electrons (>100 keV, SST Foil) and protons (>1 MeV, SST Open). We use the Wind magnetic field instrument (MFI) [*Lepping et al.*, 1995] to define the region we call the outer magnetosphere as the region between the terrestrial magnetopause and the radiation belts.

[7] The wave vector, **k**, and propagation angle with respect to the magnetic field, θ_{kB}, were determined using Minimum Variance Analysis (MVA) [*Khrabrov and Sonnerup*, 1998] on bandpass filtered TDSS samples with three magnetic field components. The frequency ranges for each bandpass filter, determined from spectral analysis, were chosen independently for each TDS sample. We required intermediate to minimum eigenvalues of the spectral matrix, $\lambda_{mid}/\lambda_{\min}$, to satisfy the condition $\geq$5.0 if less than 50 field vectors were used in the analysis [*Khrabrov and Sonnerup*, 1998]. All reported wave normal angles were calculated using MVA on three magnetic field component TDSS samples.

[8] We performed a search of 13 Wind petal orbits between 1998-11-13 and 2002-10-10, examining every TDS sample observed inside the magnetopause and within an L-shell of 15. We limited the results to L $\leq$ 15 because of the small number of TDS events at higher L-shells and difficulties in the identification of a clear magnetopause crossing. Though we observed whistler mode waves inside the magnetosphere on all 13 petal orbits, only 12 orbits had whistler mode waves inside an L-shell of 15. We define a TDS sample as a whistler mode wave when it is elliptically or circularly right-hand polarized with respect to the magnetic field and has $f_{lh} \leq f \ll f_{ce}$, where f_{lh} ($= \sqrt{f_{ce} f_{ci}}$) is the lower hybrid frequency and f_{cs} is the cyclotron frequency of species *s*. We observed 247 waveform captures identified as whistler mode waves, 191 using electric fields and 56 using magnetic fields.

3. Observations

[9] Figure 1 presents an example of a Wind perigee pass from 1998-11-13/13:00:00 UT to 1998-11-14/02:00:00 UT. The vertical black lines indicate whistler mode wave

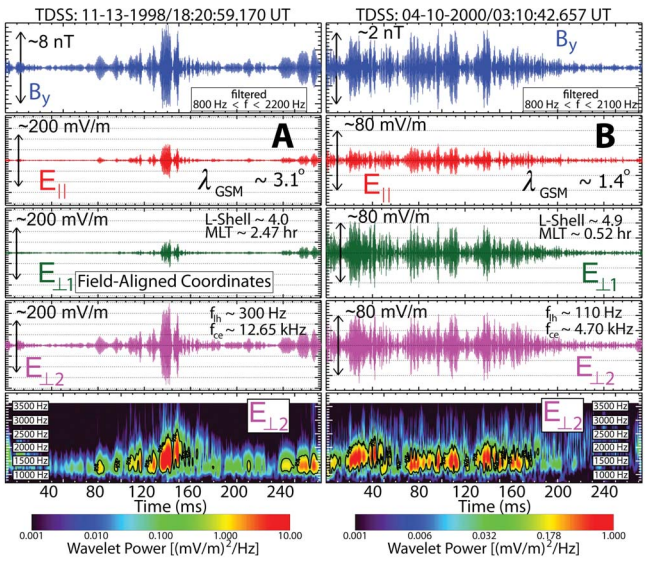

Figure 2. Examples of two whistler mode waves, single magnetic field component in instrument coordinates and electric fields in FACs, observed on the perigee passes of Wind on (a) 1998-11-13 and (b) 2000-04-10. The examples were taken from the TDSS instrument, rotated into FACs, and then we applied a standard Fourier bandpass filter (frequency range shown in first panels) to remove superposed low and high frequency signals. The first panels show the B_y (blue, instrument coordinates), second panels show $E_{||}$ (red), third panels show $E_{\perp,1}$ (green), and the fourth panels show $E_{\perp,2}$ (magenta). The fifth panels show wavelet transforms of the unfiltered $E_{\perp,2}$-component plotted on a linear frequency scale from ~700–4000 Hz, with corresponding power spectrum scale shown below [*Torrence and Compo*, 1998]. Note that the equatorial electron cyclotron frequencies for these two waves are ~12.94 kHz for the 1998-11-13 whistler mode wave and ~7.16 kHz for the 2000-04-10 event.

observations made with the TDS receiver. Figure 1 (middle and bottom) are omni-directional number fluxes of high energy electrons (SST Foil) and protons (SST Open), respectively, from the Wind/3DP instrument. The SST plots appear to show higher flux levels in the outer magnetosphere than in the radiation belts in some energy bins, but this is due to instrument saturation near perigee, causing underestimation of the fluxes between 40–182 keV for the electrons and 71–196 keV for the protons.

[10] Figure 2 plots two whistler mode waves observed near the equatorial plane, post midnight near L ~4. These whistler mode waves were obtained from the TDSS instrument (with three electric and one magnetic field components sampled at 7.5 kHz). We have used the ambient magnetic field, $\mathbf{B}_o$, and the sun direction, $\mathbf{X}_{GSE}$, to create an orthogonal field-aligned coordinate (FAC) system. The first axis is parallel to $\mathbf{B}_o$, (red, $E_{||}$ in Figure 2) and another axis is parallel to $\mathbf{B}_o/|\mathbf{B}_o| \times \mathbf{X}_{GSE}$ (magenta, $E_{\perp,2}$). The final axis (green, $E_{\perp,1}$) completes the right-handed basis. The waveforms were rotated into FACs and then we applied a standard Fourier bandpass filter (frequency range shown in Figure 2, top) to remove superposed low and high frequency signals. The L-shell, MLT, GSM latitude, f_{lh}, and the local f_{ce} for each corresponding whistler mode wave are labeled in Figure 2. Figures 2a (bottom) and 2b (bottom) show the unfiltered $E_{\perp,2}$-component wavelet transform [*Torrence and Compo*, 1998] with corresponding power spectrum with linear scale below from ~700 Hz to 4000 Hz. Note that the other electric field components and one magnetic field component show similar dynamic spectra. The frequency peak in Figure 2a appears to drift in time between 120–160 ms. However, the instrument is saturating during this interval, which contaminates multiple frequency bins in the wavelet transform. Therefore, it is difficult to determine whether the rising tone is physical or artificial. Figure 2b does not show features consistent with the typical dispersive signature of whistler mode chorus observed in previous studies [e.g., *Santolík et al.*, 2003]. We do observe some events (59/247) that have frequency peaks which clearly drift in time, but the majority do not share this trait. This is why we chose the generic name whistler mode wave.

[11] The example in Figure 2a, at 8 nT peak-to-peak, contains the largest whistler mode wave magnetic field ever reported in the magnetosphere. This amplitude results from only one component of the magnetic field, therefore the actual magnetic amplitude is likely to be larger. The electric field for this waveform saturated the instrument so the electric field peak-to-peak amplitude is also larger than the ~300 mV/m seen in the $E_{\perp,2}$-component. As one can see in the figure, the polarizations of the two perpendicular components are highly elliptical and significant fractions (>33%) of their electric field components are parallel to the ambient magnetic field, which implies that they propagate at oblique angles to the magnetic field. Such anomalously high field-aligned electric fields were recently reported by *Breneman et al.* [2011] in the inner radiation belt.

[12] Recent observations [*Kellogg et al.*, 2010; *Kersten et al.*, 2011] have shown that these large amplitude whistler mode waves can strongly interact with high energy electrons. Therefore, we use the relationship for the maximum change in kinetic energy, $(\Delta KE)_{max}$, of an electron interacting with a parallel propagating whistler derived by *Omura et al.* [2007, equation 44] to estimate the maximum kinetic energy these waves can impart to electrons. We find that the wave in Figure 2a could produce $(\Delta KE)_{max}$ ~ 61 MeV electrons, assuming propagation parallel to the magnetic field. The impact of oblique propagation on the above calculation is beyond the scope of this paper but has been addressed using the test particle simulations of *Roth et al.* [1999] in the context of the radiation belts [*Cattell et al.*, 2008; *Kersten et al.*, 2011]. Although we cannot calculate the full wave Poynting flux since we only have one electric field component for the examples in Figure 2, we can estimate a lower bound on the wave Poynting flux. We found the wave in Figure 2a had as a lower bound Poynting flux magnitude of $\gtrsim$300 μW/m^2, while the wave in Figure 2b had $\gtrsim$30 μW/m^2. Even though these estimates are lower bounds on the total Poynting flux magnitude, they are still 3–4 orders of magnitude larger than the estimates found by *Santolík et al.* [2010] (~0.05 μW/m^2), and are thus consistent with much more rapid energization of relativistic electrons. The examples show that: (1) large amplitude whistler mode waves in the radiation belts are bursty; (2) electric fields are in excess of two orders of magnitude above previous time-averaged spectral intensity observations consistent with those reported by *Cattell et al.* [2008] and *Cully et al.* [2008]; and (3) the search coil

magnetic field amplitudes exceed those of previous time-averaged spectral intensity observations by two orders of magnitude.

[13] We observed 247 whistler mode waves observed with at least one electric field component and 66 with at least one magnetic field component in our study. Of the 247 total TDS samples, 217 whistler mode waves occurred within the radiation belts. Roughly 104/191 of the whistler mode waves with two (TDSF) or three (TDSS) electric field components have peak-to-peak amplitudes $|\mathbf{E}| \geq 80$ mV/m and 28/56 of the whistler mode waves with three magnetic field components (TDSS) have $|\mathbf{B}| \geq 0.8$ nT. The mean plus or minus the standard deviation of the mean of the peak-to-peak wave amplitudes for the 191 electric field whistler mode waves were 138 ± 10 mV/m, whereas the 56 magnetic field whistler mode waves were 1.0 ± 0.2 nT. Due to the limitations of data rate and the selection criteria for the TDS, it is not possible to determine what percentage of the time these very large amplitude waves occur in the radiation belts. This question will be resolved by the upcoming RBSP mission.

[14] We observed the waves over a broad range of MLT and a small range of GSM latitudes, λ_{GSM}. We observed 73/247 whistler mode waves between 21 hrs < MLT ≤ 24 hrs and 81/247 are observed between 0 hrs ≤ MLT ≤ 3 hrs, the majority of which were inside 6 R_E in the radiation belts. We observed 114/247 waves with $|\lambda_{GSM}| \leq \pm 5°$, 52/247 with $5° < |\lambda_{GSM}| \leq 10°$, 22/247 with $10° < |\lambda_{GSM}| \leq 15°$, 50/247 with $15° < |\lambda_{GSM}| \leq 20°$, and 9/247 with $|\lambda_{GSM}| > 20°$. There were 46 TDSS samples with three magnetic field components that satisfied our criteria for the use of MVA. We found that the waves had a broad range of wave normal angles with respect to the magnetic field ($0° \leq \theta_{kB} < 50°$), where 30/46 of the waves had $\theta_{kB} \leq 20°$, 10/46 had $20° \leq \theta_{kB} \leq 30°$, and 6/46 had $\theta_{kB} > 30°$. For these 46 TDSS samples, we observed no relationship between θ_{kB} and GSM latitude.

[15] We observed the majority of the waves, 162/247, during magnetically active periods with AE >200 nT. When we examined the dependence of the wave amplitude on one minute AE-Index estimates (not shown), we found a slight increase in wave amplitude with increasing AE, consistent with previous observations [*Li et al.*, 2009]. A cursory examination of LANL geosynchronous low energy (30–300 keV) electron data shows large injections on the nightside just prior to the two whistler mode waves observed in Figure 2. Both the LANL observations of particle injections and the increasing wave amplitude with increasing AE would be consistent with increased substorm activity providing free energy for wave growth. We did observe some evidence of substorm injections in the LANL data for every orbit examined herein. However, as discussed above, we observe as nearly as many waves on the dusk side of Earth as the dawn. The observation of waves on the dusk-side is not consistent with the standard picture of wave generation by ~10–100 keV electrons injected near midnight and drifting around towards dawn [*Thomsen*, 2004].

4. Discussion and Conclusions

[16] We present a study of the properties of large amplitude whistler mode waves in the radiation belts and outer magnetosphere to provide a more detailed characterization of large amplitude whistler mode waves described by *Cattell et al.* [2008], *Cully et al.* [2008], and *Kellogg et al.* [2011]. We have also presented the largest whistler wave magnetic field (≳8 nT peak-to-peak) observations ever reported in the radiation belts, with a corresponding Poynting flux magnitude ≳300 μW/m^2, nearly four orders of magnitude above previous time-averaged spectral intensity observations. Minimum variance analysis showed that these large amplitude whistler mode waves can propagate at very oblique angles (up to ~50°) with respect to the ambient magnetic field, but 30/46 propagate within 20°.

[17] The majority of the whistler mode waves in our study were observed with frequencies less than or equal to half the local (and equatorial) electron cyclotron frequency with a mean frequency of ~1.4 ± 1.0 kHz. The mean value of the wave frequency normalized by the local(equatorial) electron cyclotron frequency is ~0.25 ± 0.17(~0.27 ± 0.26). We observed 114/247 waves with $|\lambda_{GSM}| \leq \pm 5°$, 166/247 with $|\lambda_{GSM}| \leq 10°$, and 188/247 with $|\lambda_{GSM}| \leq 15°$. Of the 247 whistler mode waves, 217 were observed in the radiation belts. We found 154/247 of the whistler mode waves to be located between 21 hrs ≤ MLT ≤ 3 hrs (i.e., nightside) while only 39/247 were between 6 hrs ≤ MLT ≤ 18 hrs (i.e., dayside). These waves have large peak-to-peak amplitudes (92/247 have ≥100 mV/m and 34/66 have ≥1.0 nT). Nearly all of the waves were observed in association with LANL low energy (30–300 keV) electron injections and 162/247 were observed during magnetically active periods (AE > 200 nT). Furthermore, the wave amplitudes show an increasing trend with increasing AE, consistent with increased substorm activity providing more free energy for whistler growth and previous observations [e.g., *Li et al.*, 2009]. However, we observed roughly an equal number of waves between 21 hrs < MLT ≤ 24 hrs (73/247) and 0 hrs ≤ MLT ≤ 3 hrs (81/247), suggesting some of the waves could not be caused by the standard model of substorm injection [*Thomsen*, 2004]. Note that the limited coverage of the Wind perigee passes make it impossible to determine the MLT distribution of the waves in a statistically meaningful way.

[18] Only recently with the introduction of waveform capture instruments have we begun to understand the range of amplitudes of whistler mode waves in the radiation belts. The largest amplitude waves were observed between 0 hrs ≤ MLT ≤ 6 hrs (i.e., dawn side), inside 6 R_E in the radiation belts, and within ±10° of the magnetic equator. We will illustrate the relative distribution of events returned by the TDS instrument by examining the two perigee passes that contain the examples shown in Figure 2, where Wind observed some of the largest whistler events ever recorded in the magnetosphere. Wind observed 11 TDSF and 3 TDSS samples consistent with whistler mode waves (in roughly 6 minutes) for the 1998-11-13 perigee pass, whereas Wind observed 27 TDSF and 7 TDSS samples (in roughly 1.75 hours) for the 2000-04-10 perigee pass. All 14 TDS samples for the 1998-11-13 perigee pass had peak-to-peak amplitudes $|\mathbf{E}| \geq$ 200 mV/m and all 3 TDSS samples had $|\mathbf{B}| \geq 8$ nT. Of the 34 TDS samples observed in the 2000-04-10 perigee pass, 31 had peak-to-peak amplitudes $|\mathbf{E}| \geq 160$ mV/m and all 7 TDSS samples had $|\mathbf{B}| \geq 2$ nT. These results are consistent with STEREO [*Cattell et al.*, 2008; *Breneman et al.*, 2011] and THEMIS [*Cully et al.*, 2008] studies. *Cattell et al.* [2008] observed 24 waveform captures with whistler mode waves in ~4 minutes all with peak-to-peak amplitudes ≥200 mV/m.

Breneman et al. [2011] examined four perigee passes by the STEREO spacecraft through the plasmasphere observing over 100 whistler mode waves with average amplitudes ≥55 mV/m and maximum peak-to-peak amplitudes ~300 mV/m. *Cully et al.* [2008], during a four day period, reported observing 85 large amplitude (many tens to hundreds of mV/m) waveform burst captures by the THEMIS spacecraft in the radiation belts. Although characterizing the detailed distributions of amplitudes will require the instrumentation available on the upcoming RBSP satellites, we argue that these large amplitude whistler mode waves may not be an uncommon phenomena. Our study adds to the mounting evidence that very large amplitude whistler mode waves are an important phenomena in the radiation belts.

[19] **Acknowledgments.** We thank R. Lin (3DP), K. Ogilvie (SWE), R. Lepping (MFI), and E. Dors (LANL data) for the use of data from their instruments. We would also like to thank M. Pulupa, S.D. Bale, and P. Schroeder for technical help with the 3DP software and analysis. We thank L. Wang for help in calibration of the SST Foil data. The authors thank World Data Center for Geomagnetism, Kyoto, for providing the AE index. This research was supported by NESSF grant NNX07AU72H, grant NNX07AI05G, the Dr.Leonard Burlaga/Arctowski Medal Fellowship, and a contract from APL for the development of RBSP/EFW.

[20] The Editor thanks two anonymous reviewers for their assistance in evaluating this paper.

References

Bell, T. F., and H. D. Ngo (1990), Electrostatic lower hybrid waves excited by electromagnetic whistler mode waves scattering from planar magnetic-field-aligned plasma density irregularities, *J. Geophys. Res.*, *95*, 149–172, doi:10.1029/JA095iA01p00149.

Bortnik, J., R. M. Thorne, and U. S. Inan (2008), Nonlinear interaction of energetic electrons with large amplitude chorus, *Geophys. Res. Lett.*, *35*, L21102, doi:10.1029/2008GL035500.

Bougeret, J.-L., et al. (1995), Waves: The radio and plasma wave investigation on the Wind spacecraft, *Space Sci. Rev.*, *71*, 231–263, doi:10.1007/BF00751331.

Breneman, A., C. Cattell, J. Wygant, K. Kersten, L. B. Wilson III, S. Schreiner, P. J. Kellogg, and K. Goetz (2011), Large-amplitude transmitter-associated and lightning-associated whistler waves in the Earth's inner plasmasphere at $L < 2$, *J. Geophys. Res.*, *116*, A06310, doi:10.1029/2010JA016288.

Burtis, W. J., and R. A. Helliwell (1969), Banded chorus: A new type of VLF radiation observed in the magnetosphere by OGO 1 and OGO 3, *J. Geophys. Res.*, *74*, 3002–3010, doi:10.1029/JA074i011p03002.

Cattell, C., et al. (2008), Discovery of very large amplitude whistler-mode waves in Earth's radiation belts, *Geophys. Res. Lett.*, *35*, L01105, doi:10.1029/2007GL032009.

Cully, C. M., J. W. Bonnell, and R. E. Ergun (2008), THEMIS observations of long-lived regions of large-amplitude whistler waves in the inner magnetosphere, *Geophys. Res. Lett.*, *35*, L17S16, doi:10.1029/2008GL033643.

Hoppe, M. M., C. T. Russell, L. A. Frank, T. E. Eastman, and E. W. Greenstadt (1981), Upstream hydromagnetic waves and their association with backstreaming ion populations: ISEE 1 and 2 observations, *J. Geophys. Res.*, *86*, 4471–4492, doi:10.1029/JA086iA06p04471.

Horne, R. B., S. A. Glauert, and R. M. Thorne (2003), Resonant diffusion of radiation belt electrons by whistler-mode chorus, *Geophys. Res. Lett.*, *30*(9), 1493, doi:10.1029/2003GL016963.

Horne, R. B., R. M. Thorne, S. A. Glauert, J. M. Albert, N. P. Meredith, and R. R. Anderson (2005), Timescale for radiation belt electron acceleration by whistler mode chorus waves, *J. Geophys. Res.*, *110*, A03225, doi:10.1029/2004JA010811.

Kellogg, P. J., C. A. Cattell, K. Goetz, S. J. Monson, and L. B. Wilson III (2010), Electron trapping and charge transport by large amplitude whistlers, *Geophys. Res. Lett.*, *37*, L20106, doi:10.1029/2010GL044845.

Kellogg, P. J., C. A. Cattell, K. Goetz, S. J. Monson, and L. B. Wilson III (2011), Large Amplitude whistlers in the magnetosphere observed with wind-waves, *J. Geophys. Res.*, doi:10.1029/2010JA015919, in press.

Kennel, C. F., and H. E. Petschek (1966), Limit on stably trapped particle fluxes, *J. Geophys. Res.*, *71*, 1–28, doi:10.1029/JZ071i001p00001.

Kersten, K., C. A. Cattell, A. Breneman, K. Goetz, P. J. Kellogg, J. R. Wygant, L. B. Wilson III, J. B. Blake, M. D. Looper, and I. Roth (2011), Observation of relativistic electron microbursts in conjunction with intense radiation belt whistler-mode waves, *Geophys. Res. Lett.*, *38*, L08107, doi:10.1029/2011GL046810.

Khrabrov, A. V., and B. U. Ö. Sonnerup (1998), Error estimates for minimum variance analysis, *J. Geophys. Res.*, *103*, 6641–6651, doi:10.1029/97JA03731.

Lepping, R. P., et al. (1995), The Wind magnetic field investigation, *Space Sci. Rev.*, *71*, 207–229, doi:10.1007/BF00751330.

Li, W., R. M. Thorne, V. Angelopoulos, J. Bortnik, C. M. Cully, B. Ni, O. LeContel, A. Roux, U. Auster, and W. Magnes (2009), Global distribution of whistler-mode chorus waves observed on the THEMIS spacecraft, *Geophys. Res. Lett.*, *36*, L09104, doi:10.1029/2009GL037595.

Lin, R. P., et al. (1995), A three-dimensional plasma and energetic particle investigation for the Wind spacecraft, *Space Sci. Rev.*, *71*, 125–153, doi:10.1007/BF00751328.

Lyons, L. R., R. M. Thorne, and C. F. Kennel (1972), Pitch-angle diffusion of radiation belt electrons within the plasmasphere, *J. Geophys. Res.*, *77*, 3455–3474, doi:10.1029/JA077i019p03455.

McFadden, J. P., et al. (2007), In-flight instrument calibration and performance verification, *ISSI Sci. Rep. Ser.*, *7*, 277–385.

Meredith, N. P., R. B. Horne, and R. R. Anderson (2001), Substorm dependence of chorus amplitudes: Implications for the acceleration of electrons to relativistic energies, *J. Geophys. Res.*, *106*, 13,165–13,178, doi:10.1029/2000JA900156.

Neubauer, F. M., G. Musmann, and G. Dehmel (1977), Fast magnetic fluctuations in the solar wind: Helios 1, *J. Geophys. Res.*, *82*, 3201–3212, doi:10.1029/JA082i022p03201.

Omura, Y., N. Furuya, and D. Summers (2007), Relativistic turning acceleration of resonant electrons by coherent whistler mode waves in a dipole magnetic field, *J. Geophys. Res.*, *112*, A06236, doi:10.1029/2006JA012243.

Roth, I., M. Temerin, and M. K. Hudson (1999), Resonant enhancement of relativistic electron fluxes during geomagnetically active periods, *Ann. Geophys.*, *17*, 631–638, doi:10.1007/s005850050791.

Santolík, O., D. A. Gurnett, J. S. Pickett, M. Parrot, and N. Cornilleau-Wehrlin (2003), Spatio-temporal structure of storm-time chorus, *J. Geophys. Res.*, *108*(A7), 1278, doi:10.1029/2002JA009791.

Santolík, O., J. S. Pickett, D. A. Gurnett, J. D. Menietti, B. T. Tsurutani, and O. Verkhoglyadova (2010), Survey of Poynting flux of whistler mode chorus in the outer zone, *J. Geophys. Res.*, *115*, A00F13, doi:10.1029/2009JA014925.

Thomsen, M. F. (2004), Why Kp is such a good measure of magnetospheric convection, *Space Weather*, *2*, S11004, doi:10.1029/2004SW000089.

Torrence, C., and G. P. Compo (1998), A practical guide to wavelet analysis, *Bull. Am. Meteorol. Soc.*, *79*, 61–78, doi:10.1175/1520-0477(1998)079.

Tsurutani, B. T., R. M. Thorne, E. J. Smith, J. T. Gosling, and H. Matsumoto (1987), Steepened magnetosonic waves at comet Giacobini-Zinner, *J. Geophys. Res.*, *92*, 11,074–11,082, doi:10.1029/JA092iA10p11074.

Tsurutani, B. T., O. P. Verkhoglyadova, G. S. Lakhina, and S. Yagitani (2009), Properties of dayside outer zone chorus during HILDCAA events: Loss of energetic electrons, *J. Geophys. Res.*, *114*, A03207, doi:10.1029/2008JA013353.

Wilson, L. B., III, C. A. Cattell, P. J. Kellogg, K. Goetz, K. Kersten, J. C. Kasper, A. Szabo, and K. Meziane (2009), Low-frequency whistler waves and shocklets observed at quasi-perpendicular interplanetary shocks, *J. Geophys. Res.*, *114*, A10106, doi:10.1029/2009JA014376.

A. Breneman, C. A. Cattell, K. Goetz, P. J. Kellogg, K. Kersten, and J. R. Wygant, School of Physics and Astronomy, University of Minnesota, Twin Cities, 116 Church St. SE, Minneapolis, MN 55455, USA. (awbrenem@gmail.com; cattell@fields.space.umn.edu; goetz@waves.space.umn.edu; pauljkellogg@gmail.com; kkersten@physics.umn.edu; jwygant@fields.space.umn.edu)

L. B. Wilson III, NASA Goddard Space Flight Center, Code 672, Bldg. 21, Room 143A, Greenbelt, MD 20771, USA. (lynn.b.wilsoniii@gmail.com)